Published in Journal of Hydrology 545, 109-119, 2017
which should be used for any reference to this work

On the use of multiple-point statistics to improve groundwater flow modeling in karst aquifers: A case study from the Hydrogeological Experimental Site of Poitiers, France

Mathieu Le Coz [a,*], Jacques Bodin [a], Philippe Renard [b]

[a] Université de Poitiers, CNRS, UMR 7285 IC2MP, 40 Avenue du Recteur Pineau, 86022 Poitiers Cedex, France
[b] University of Neuchâtel, Centre for Hydrogeology and Geothermics, 11 Rue Emile Argand, CH-2000 Neuchâtel, Switzerland

Keywords:
Pumping tests
Heterogeneous media
Karst conduit network simulation
Reservoir

A B S T R A C T

Limestone aquifers often exhibit complex groundwater flow behaviors resulting from depositional heterogeneities and post-lithification fracturing and karstification. In this study, multiple-point statistics (MPS) was applied to reproduce karst features and to improve groundwater flow modeling. For this purpose, MPS realizations were used in a numerical flow model to simulate the responses to pumping test experiments observed at the Hydrogeological Experimental Site of Poitiers, France. The main flow behaviors evident in the field data were simulated, particularly (i) the early-time inflection of the drawdown signal at certain observation wells and (ii) the convex behavior of the drawdown curves at intermediate times. In addition, it was shown that the spatial structure of the karst features at various scales is critical with regard to the propagation of the depletion wave induced by pumping. Indeed, (i) the spatial shape of the cone of depression is significantly affected by the karst proportion in the vicinity of the pumping well, and (ii) early-time inflection of the drawdown signal occurs only at observation wells crossing locally well-developed karst features.

1. Introduction

The spatial heterogeneity of geologic media exerts a significant influence on groundwater flow and the associated transport from the subpore scale up to the regional scale. The arrangement of discrete structures, such as faults, fractures, dissolution conduits and coarse-grained channel fills, often characterizes the first-order heterogeneity, i.e., the most hydrologically significant heterogeneity, because the bounding surfaces between these structures mark discontinuities in hydrodynamic property fields (Ronayne et al., 2008; Bianchi et al., 2015). Particular attention must be paid to connected structures that form high-diffusivity flow paths or low-diffusivity flow barriers, which can result in concentrations of water flux in small portions of the domain and consequently in a significant increase in average flow rates and an even more significant reduction in the first arrival times of contaminants (Knudby and Carrera, 2006). Identifying and modeling the influence of these dominant structures at relevant scales represent a key research challenge (Noushabadi et al., 2011; Lee and Kitanidis, 2013; dell'Arciprete et al., 2014).

In limestone formations, the preferential dissolution of calcite along horizons with pre-existing discontinuities (e.g., bedding planes and fractures) can lead to the evolution of complex networks, often spanning several kilometers through the limestone matrix (Filipponi et al., 2009). A number of studies have addressed the characterization and simulation of such networks using various tools, the choice of which depends on both the scale under consideration and the available data, e.g., (i) genetic models that simulate speleogenesis processes based on the prevailing paleoclimatic and ecological conditions during karst formation (Kaufmann and Braun, 2000), (ii) conceptual models that generate karst conduits from inlets to outlets by running a random walk algorithm within a limestone matrix for which the fracturing and bedding planes have been previously described (Borghi et al., 2012), and (iii) geostatistical models that simulate conduits in accordance with geometric properties measured from analogs (Fournillon et al., 2010). However, such geostatistical models are generally based on two-point spatial statistics, which can be insufficient for appropriately capturing the connectivity of karst conduits and thus for producing realistic networks (Renard and Allard, 2013).

Multiple-point statistics (MPS) enables the generation of complex, curvilinear, continuous, or interconnected geological structures in a stochastic framework (Strebelle, 2002; Huysmans and

* Corresponding author.
E-mail address: mathieu.lecoz@univ-poitiers.fr (M. Le Coz).

Dassargues, 2011; Straubhaar et al., 2011). MPS overcomes the limitations of the variogram approach through the direct inference of the necessary multivariate distributions from training images (Huysmans and Dassargues, 2012). In the field of groundwater hydrology, the application of MPS to the modeling of groundwater flow and transport in heterogeneous media has become an active area of research in recent years (Ronayne et al., 2008; Le Coz et al., 2011; dell'Arciprete et al., 2012; Huysmans and Dassargues, 2012). To the best of the authors' knowledge, the only study reporting the use of MPS in karst flow models was presented by Balan (2012), who integrated MPS-simulated cave networks into a petroleum reservoir model and analyzed the resulting simulated oil production profiles over a long period of time (40 years). In the present study, we investigate the applicability of MPS for groundwater flow modeling in karst aquifers. More precisely, we assess the relevance of MPS for improving the simulation of the complex drawdown responses observed at short and moderate time scales in a well-studied karst aquifer.

In Section 2, the variety of hydraulic responses to flow experiments performed in the Dogger aquifer at the Hydrogeological Experimental Site (HES) of Poitiers (in west-central France) is described. In Section 3, MPS is applied to simulate karst-induced aquifer heterogeneities, and the resulting images are used as inputs to a groundwater flow model. In Sections 4 and 5, the ability of the model to reproduce the observed hydraulic behaviors is described and discussed.

2. Hydraulic behaviors in a karstified limestone aquifer

The HES is a facility maintained by the University of Poitiers for the sole purpose of research and engineering development. The high density of wells available for groundwater surveys within a limestone aquifer enables the observation of various typical hydraulic head responses to flow experiments. These responses were interpreted with regard to the strong aquifer heterogeneity induced predominantly by the presence of karst features.

2.1. The HES

The HES is located within a geological area called "The Poitou Threshold", which marks the transition between two large Mesozoic-Cenozoic sedimentary basins: the Paris basin to the North and the Aquitaine basin to the South (Fig. 1). The Poitou Threshold is composed of a series of Jurassic carbonates overlapping a Hercynian-orogeny-related basement of crystalline rocks. Two limestone aquifers of regional extent are present in the Jurassic carbonate series, from bottom to top, as follows: (i) the lower and middle Lias aquifer (from 5 m to 200 m thick) and (ii) the Dogger aquifer (from 50 m to 200 m thick). These two aquifers are separated by a Toarcian marl aquitard (from 5 m to 20 m thick). Most of the investigations performed at the HES target the Dogger aquifer, which is 100 m thick in this region and is confined beneath 10–25 m of Tertiary clays.

The HES includes 32 fully penetrating wells that were drilled in two separate phases, in 2002–2003 and 2004, down to the Dogger aquifer basement. The majority of the wells are spatially distributed as nested five-spots (an elementary pattern consisting of four wells at the corners of a square and one at the center) within a square area of 210 m × 210 m (Fig. 2(a)) and are either fully screened or open over the entire thickness of the aquifer.

The permeability structure of the aquifer has been extensively characterized over the past decade through hydrogeophysical well logging (Audouin et al., 2008; Chatelier et al., 2011) and 3D seismic surveying (Mari and Porel, 2008; Mari et al., 2009). The data indicate that the flow paths in the aquifer are strongly constrained within sub-horizontal karst conduits, 0.01–3 m in diameter, that develop preferentially within specific lithostratigraphic horizons interbedded with nonkarstified limestone units. More precisely, three thin (from 2 m to 5 m thick) karstified horizons were identified within the 100-m-thick Dogger limestone formation. At the HES scale, these levels are sub-horizontal (dip less than 2°) and are located at depths of approximately 30 m, 80 m and 110 m. Each of these karstified layers contributes to the connectivity from one well to another, either directly (the two wells intersect with the same network) or indirectly (the two wells intersect with two distinct networks, which are both intersected by either a third well or a sub-vertical fracture).

2.2. Hydraulic head responses to flow experiments

Several pumping test experiments have been conducted at the HES since 2002. For each test, a constant pumping rate ranging from $1 \times 10^{-2}\ m^3\ s^{-1}$ to $2 \times 10^{-2}\ m^3\ s^{-1}$ was prescribed over a long time period, up to 6×10^5 s. The measured drawdown curves exhibit various behaviors in space depending on both the pumped and observed wells. To illustrate the most representative behaviors, drawdown curves corresponding to pumping tests performed in wells M12 and M06 are described below. For the sake of later comparison with the numerical simulations discussed in Section 4, these experimental drawdown curves have been linearly rescaled based on a pumping rate of $2 \times 10^{-2}\ m^3\ s^{-1}$.

For the pumping test experiment at well M12, it is observed that (i) at the majority of the observation wells (Fig. 3(a)), an oscillatory response occurs within the first 100 s, inflection of the drawdown curves appears between 10 s and 100 s, and the drawdown curves are generally close in both time and amplitude beyond 100 s; (ii) at observation wells M03, M06, M09, M11, M17 and MP7 (Fig. 3(b)), neither oscillation nor inflection occurs at early times, but the drawdown curves remain similar to the previous ones in time and amplitude beyond 100 s; (iii) at observation wells M08, M10, M14 and M18 (Fig. 3(c)), neither oscillation nor inflection occurs, and the response time is significantly delayed (by approximately 10^3 s) with respect to the other observation wells, resulting in lower amplitudes of the drawdown signals; and (iv) at all observation wells (Fig. 4(a–c)), the drawdown curves are convex at intermediate times (10^3–10^4 s) and over long periods, i.e., the drawdown increases more rapidly than linearly with the natural logarithm of time.

For the pumping test experiment at well M06, it is observed that (i) at the majority of the observation wells (Fig. 3(d, e)), neither oscillation nor inflection occurs, and the drawdown curves are close in both time and amplitude beyond 100 s; (ii) at observation wells M03, M04, M06 and M11 (Fig. 4(d, e)), the amplitude of the responses is significantly higher, and inflection of the drawdown curves occurs at approximately 10^3 s; (iii) at observation wells M08, M10, M14 and M18 (Fig. 3(d)), neither oscillation nor inflection occurs, and the response time is significantly delayed (by approximately 10^3 s), resulting in lower amplitudes of the drawdown signals; and (iv) at all observation wells (Fig. 4(a–c)), the drawdown curves are convex at intermediate times and over long periods.

2.3. Assumptions about hydraulic behaviors

Of the 25 wells involved in the two pumping test data sets described in Section 2.2, the 21 wells that show rapid drawdown responses actually intercept one or two karst conduits, as indicated by flowmeter and borehole image logging (Audouin et al., 2008). Likewise, the oscillatory responses observed in certain observation wells at early times are typical of high hydraulic conductivities (Butler and Zhan, 2004) and correspond to wells that are indeed

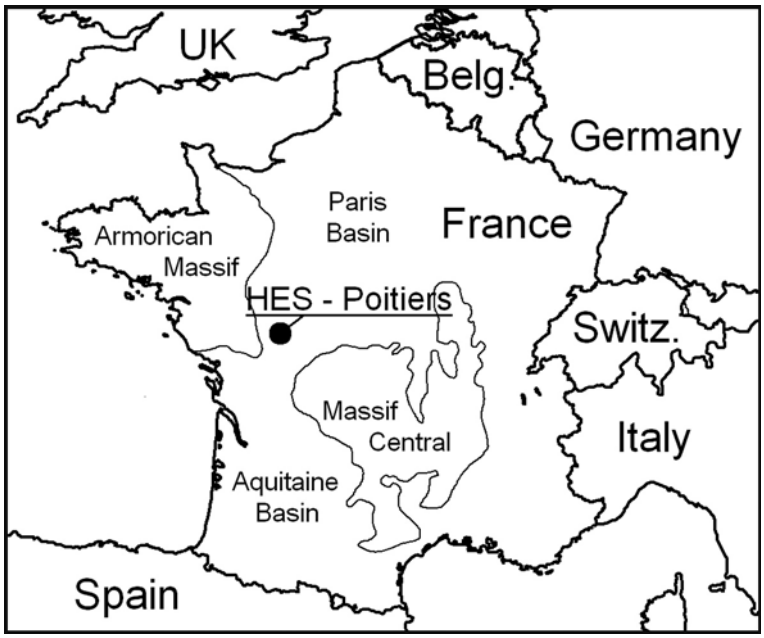

Fig. 1. Location of the Hydrogeological Experimental Site (HES) in France.

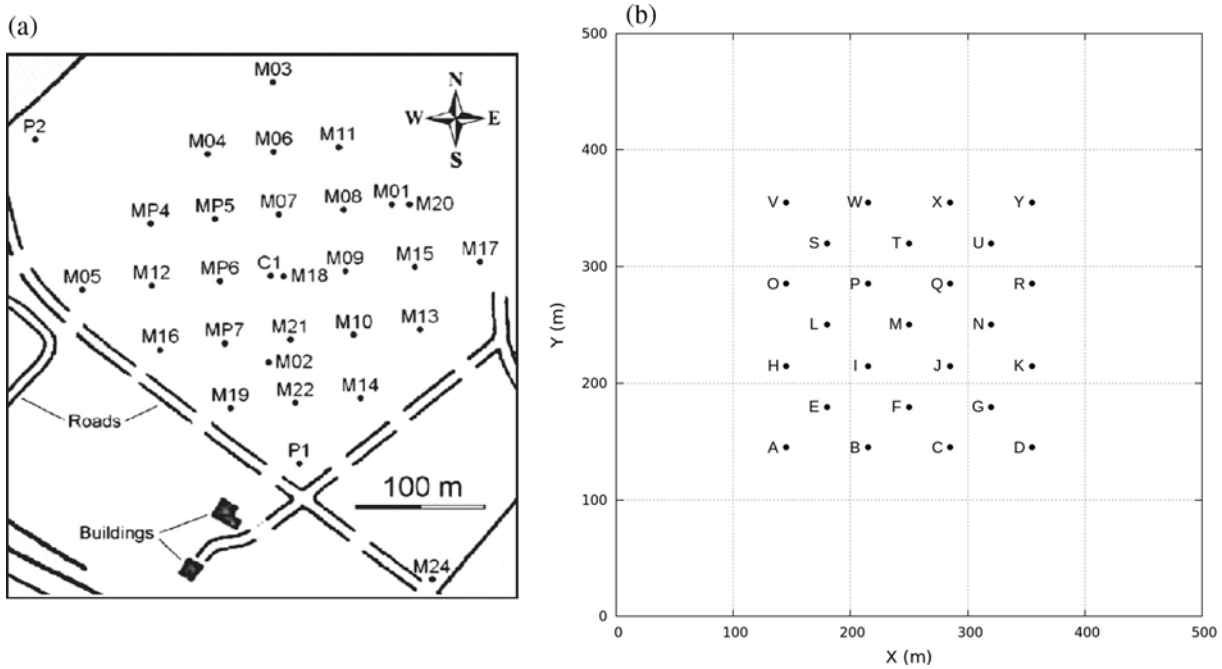

Fig. 2. Locations of the wells at the HES (a) and within the modeling domain (not constrained by field data) (b); in both configurations, the wells are distributed as nested five-spots (an elementary pattern consisting of four wells at the corners of a square and one at the center) of 70 × 70 m within a square area of 210 × 210 m.

well connected to the pumping well through highly permeable flow paths. At these same observation wells, the inflection of the drawdown curves at early times, which is commonly interpreted as a behavioral signature of a dual-porosity medium, could correspond to the transition between the rapid drainage of the initial water content of the karst networks and the progressive feeding of water by the porous matrix (Kaczmaryk and Delay, 2007a). Moreover, the quasi-similarity of these drawdown curves regardless of the lag distance (for a given pumping experiment) indicates that the depletion wave due to pumping is able to propagate very rapidly, resulting in no significant difference in the response times (Kaczmaryk and Delay, 2007b).

The significant delays in the response times at observation wells M08, M10, M14 and M18 (Fig. 3(c, f)) could be explained by the fact that these wells do not intersect with the karst networks, as indicated by flowmeter and borehole image logging (Audouin et al., 2008). Therefore, to reach these wells, the depletion wave must pass through the porous matrix, which is characterized by a relatively low hydraulic diffusivity. The porous matrix also functions as a buffer zone that smooths both

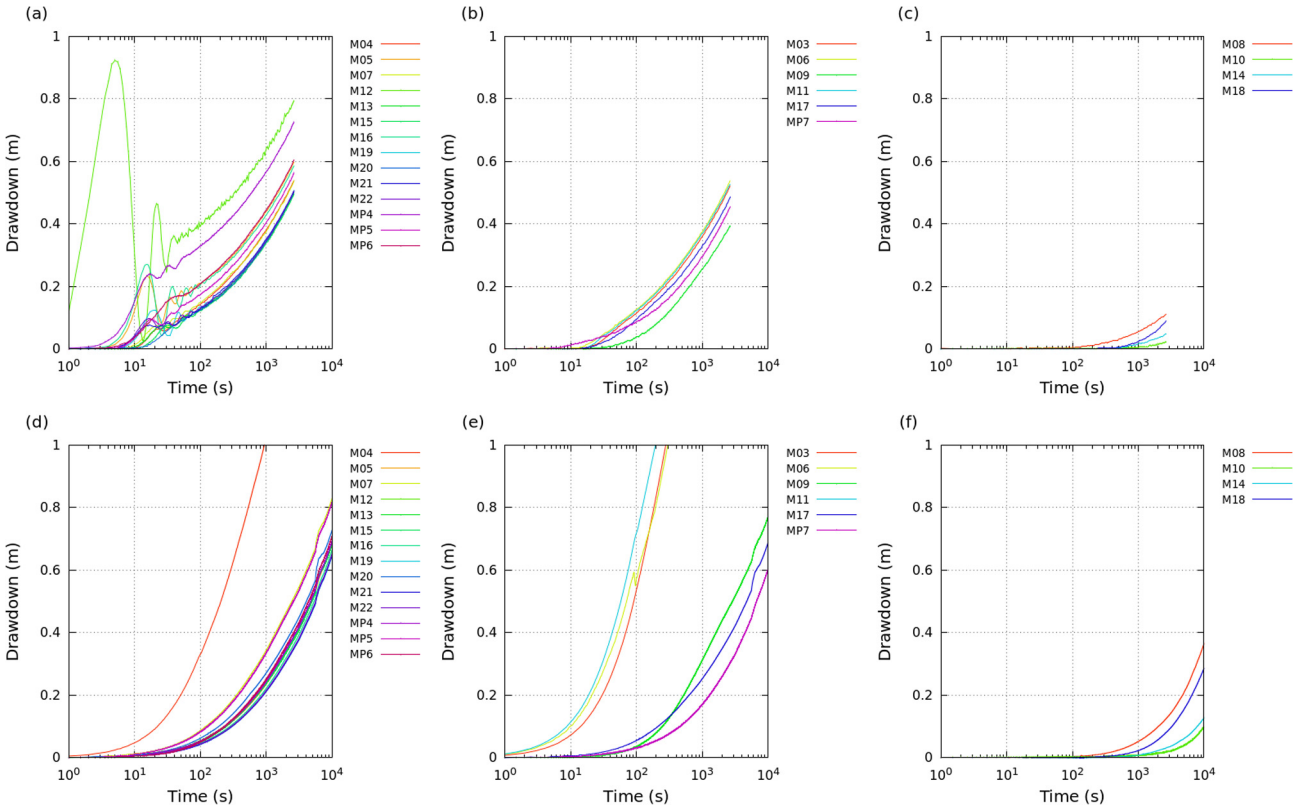

Fig. 3. Equivalent (scaled) drawdown observations at early to intermediate times during the pumping test experiments performed at wells M12 (a–c) and M06 (d–f); the drawdown scaling was performed based on a pumping rate of 2×10^{-2} m^3 s^{-1}.

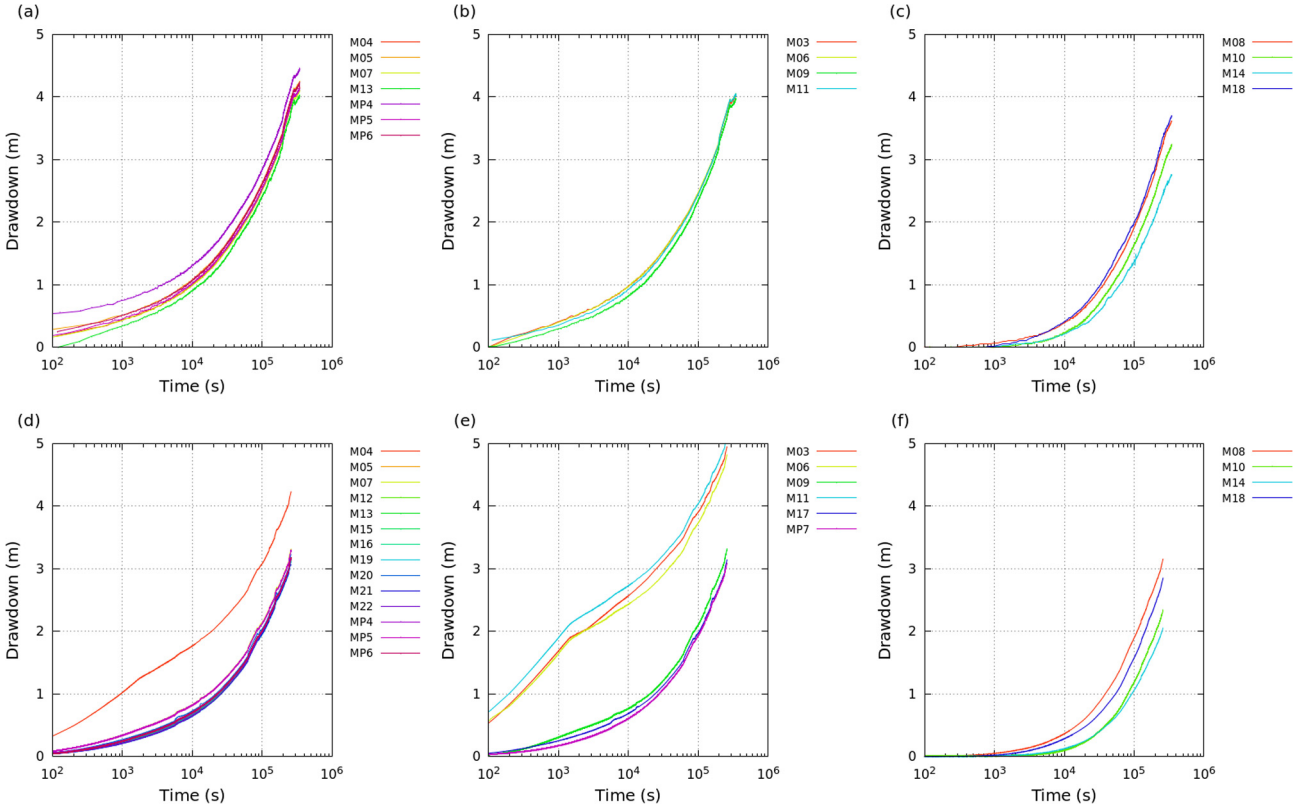

Fig. 4. Equivalent (scaled) drawdown observations at intermediate to late times during the pumping test experiments performed at wells M12 (a–c) and M06 (d–f); the drawdown scaling was performed based on a pumping rate of 2×10^{-2} m^3 s^{-1}.

oscillations and inflections of the drawdown signal. The drawdown responses at observation wells M03, M06, M09, M11, M17 and MP7 (Fig. 3(b, e)) are also affected by such smoothing but do not exhibit any delay in arrival time that could indicate locally specific medium structures or hydraulic properties.

The convex behavior observed at intermediate and late times has been interpreted as a possible result of fractal heterogeneity in the aquifer properties (Bernard et al., 2006; Kaczmaryk and Delay, 2007a), and the parameters obtained through the inversion of fractal flow models have been discussed in terms of the homogenization scale as a transition from a typically three-dimensional flow at early times to a two-dimensional flow at later times.

3. Modeling approach

3.1. General methodology and assumptions

A basic issue in any spatially distributed modeling approach is the choice of model dimensionality. In the present case, although a 3D modeling approach might have been considered to describe both the horizontal and vertical heterogeneity of the aquifer, we deliberately chose to perform 2D simulations. The rationale is that we consider the vertical heterogeneity of the aquifer to be negligible with respect to its horizontal heterogeneity. This assumption is supported by (i) the specific hydrogeological structure of the aquifer, which is formed by 3 thin (from 2 to 5 m thick) sub-horizontal karstified limestone horizons embedded within a 100-m-thick non-karstified limestone matrix (see Section 2.1), and by (ii) the previous flow modeling studies of the HES, including a comparison between several 2D and 3D models (Bodin et al., 2012), which indicated no significant advantage of 3D approaches in terms of calibration and predictive modeling capabilities.

The MPS method was thus used to simulate 2D "equivalent-m erged" karst networks that aim to capture the HES interwell connectivity structure, which is actually distributed among the three sub-horizontal karst horizons. The simulated karst network images were then used to map the spatial heterogeneity of aquifer hydraulic properties according to either a "karst facies" or a "non-karstified rock facies", with each facies being associated with a range of hydraulic property values identified from previous independent studies (see Section 3.2).

The training image used for the MPS simulations (Fig. 5(a)) is the map of a cave system located in the Cuchon Valley, 10 km east of the HES. This cave develops in the same geological unit (i.e., the same stratigraphy unit and sedimentary facies) as the karst layers identified at the HES. The cave conduit network covers an overall area of 350 m $\times$ 350 m and is mainly sub-horizontal to gently dipping upward in the northern part of the cave. Most cave conduit elevations vary from +5 m to -5 m around the mean elevation plane. Only a few passages (e.g., the pit entrance or local deep points) diverge up to +20 m to -10 m. Because of the overall horizontality of the Cuchon Valley cave and its geological analogy with the HES, the 2D projection of the cave survey is assumed to be representative of the spatial structure (conduit orientation, tortuosity, correlation length) of the karst flow paths in the Dogger aquifer. This 2D projection was used for MPS training using the IMPALA algorithm (Straubhaar et al., 2011).

A typical issue with MPS is spatially non-stationary data. Stationarity is indeed a theoretical prerequisite both for deriving the multiple-point probability distributions from the assumed consistent replication of heterogeneity patterns within the training image and for exporting these statistics to the simulated realizations (Strebelle and Zhang, 2005). Because the stationary assumption may not be valid for real-world geological datasets, some techniques have been developed to circumvent this problem. The idea is to add further probability control to the MPS simulations through the use of one or several maps of continuous auxiliary variable(s) for describing non-stationarity (Chugunova and Hu, 2008; Straubhaar et al., 2011). A quick look at the cave conduit network proposed as a training image in the present work shows that the stationarity assumption is invalid here (Fig. 5(a)). The strategy should therefore be to apply the above-mentioned specific techniques. However, due to the scarcity of available karst geometry data within the study area, a rigorous characterization of the non-stationarity is unfortunately impossible, i.e. we don't have local information about the non-stationarity. Since the Cuchon Valley cave conduit network is the only available training image, we deliberately chose to perform 2D MPS simulations from this unique non-stationary training image (aware of the fact that TIs should be stationary).

Another challenge raised by our approach is that of karst conduit network density. Because the simulated 2D karst networks are aimed at gathering flow paths that are actually distributed among three superposed karst horizons, the density of the simulated conduit networks must be higher than that of the real "single layer" karst networks (such as that depicted by the training image). The karst network density in the MPS-simulated images was therefore treated as a calibration parameter with calibration being performed against the HES well interconnectivity inferred from pumping test data (see Section 3.2). To modify the density of karst networks we provided different global proportion targets to IMPALA. For each pixel during the sequential simulation, the algorithm updates the local conditional probability density function derived from the training image by combining it with the target proportion using Bordley's formula (Allard et al., 2012).

As direct consequences of the two above-mentioned modeling choices (namely, the use of a non stationary training image and modification of the karst density in the MPS simulations), the simulated karst networks are not expected to "resemble" the training image, and statistical comparisons between the TI and simulated images would have no meaning. However, we believe that these items are not of real concern because they do not represent the primary purpose of this study, which is rather to seek 2D "effective" karst networks while instilling some part of the training image conduit network patterns to the MPS-simulated networks. The relevancy of this approach will be a posteriori assessed regarding its ability to reproduce the observed hydraulic behaviors within a groundwater modeling framework (see Section 3.3).

3.2. Karst network density and hydrodynamic properties

Based on the statistics derived from the training image, 2D binary images were simulated within an area of 200 m in radius, i.e., the size of the HES, with a 1 m $\times$ 1 m spatial resolution and an adjustable proportion of "karst facies" (value = 1) versus the "non-karstified rock facies" (value = 0) (Fig. 5(b–d)). A circular outline of the MPS realizations was chosen because of the radial nature of the pumping test experiments analyzed and simulated in the present study. The calibration of the karst network proportion was based on the HES well interconnectivity inferred from the drawdown data sets illustrated in Figs. 3 and 4. The total number of wells involved in these data sets, including both the pumping wells and the observation wells, is 25. As discussed in Section 2.3, 21 of these 25 wells were shown to be well interconnected through high-permeability karst flow paths, whereas 4 wells (M08, M10, M14 and M18) only intercept non-karstified limestones. To identify the karst network proportion consistent with this 21:25 well-interconnectivity ratio, the following procedure was applied: (i) sets of 100 MPS images were simulated with various karst network proportions; (ii) 25 well locations were added to the images according to a regular pattern, as illustrated in Fig. 2(b) and

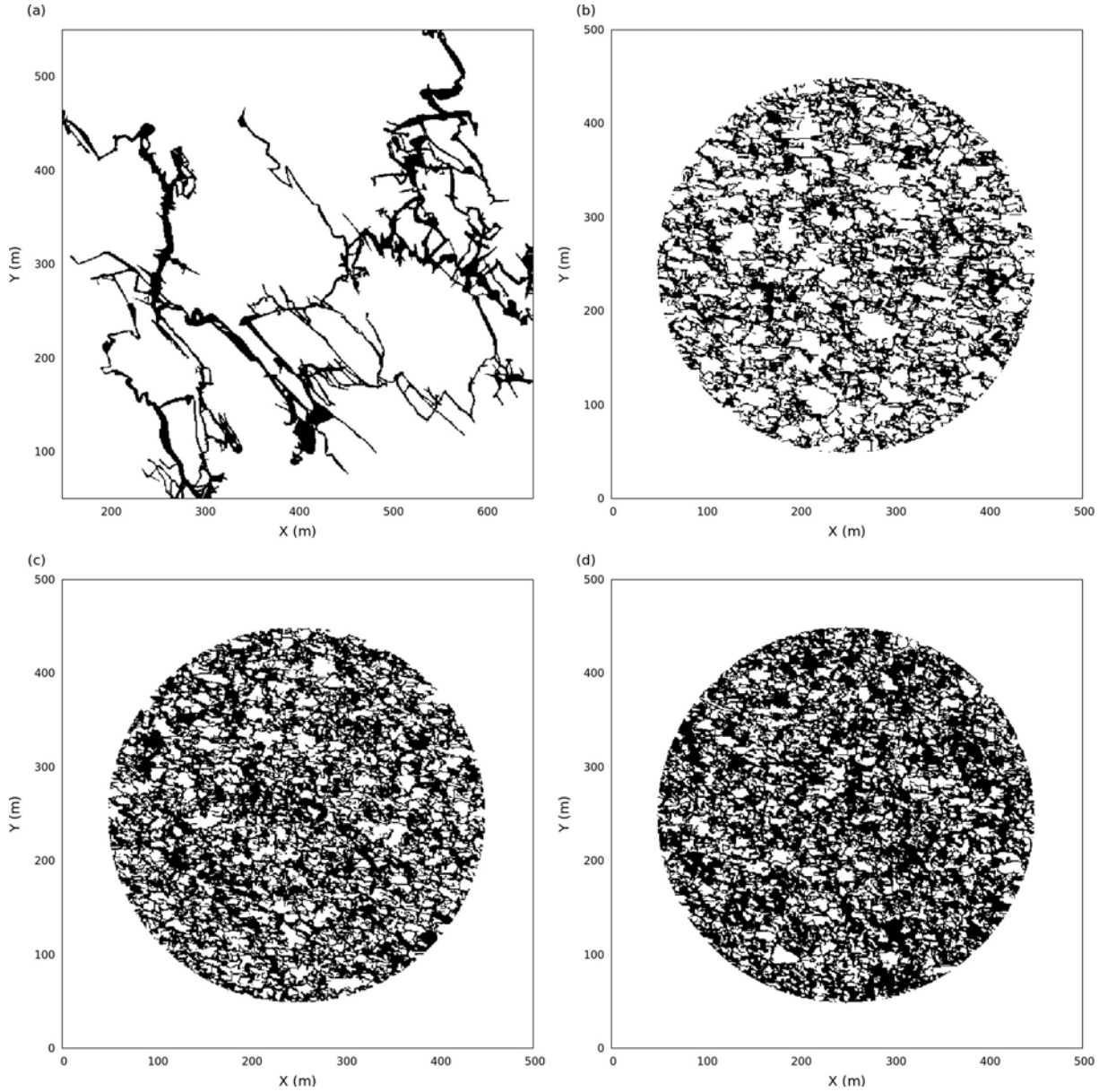

Fig. 5. Binarized speleological map used for MPS training (Cuchon cavern, Chauvigny, France; the karst channels are mapped in black) (a) and MPS realizations with karst network proportions of 40% (b), 55% (c) and 65% (d). Visually, the simulated images differ from the training image because of (i) their significantly higher karst network proportions and (ii) the absence of constraints governing the spatial variation in the probability of karst network occurrence.

consistent with the spatial arrangement of the HES wells (Fig. 2 (a)); and (iii) MPS realizations were scanned with an 8-connected neighborhood kernel (i.e., two karst pixels with a common side or a common corner are considered to be connected together) to establish a relationship between the karst proportion and the number of wells interconnected through a continuous pathway of karst pixels. As shown in Fig. 6, the karst network proportion that corresponds to a 21:25 well interconnectivity ratio ranges between 45% and 65%.

Approximately 150 drawdown curves from nine pumping test experiments performed at the HES since 2005 have been interpreted using various deterministic and stochastic approaches (Bodin et al., 2012). Most of these approaches focus on intermediate to late times, and the resulting hydraulic properties are therefore assumed to be representative of the bulk aquifer material. The transmissivity and storage coefficient values obtained using the different interpretation methods range from $6 \times 10^{-4}\,m^2\,s^{-1}$ to $3 \times 10^{-2}\,m^2\,s^{-1}$ and from 4×10^{-5} to 3×10^{-1}. In addition, a series of 66 cross-borehole slug test experiments were conducted to support the 2005 pumping test campaign. Whereas pumping tests involve the entire karst/matrix system because of the limited storage of a karst network, the hydraulic head perturbation induced by slug tests propagates only through the flow paths of least resistance, i.e., the karst network (Bodin et al., 2012). The cross-borehole slug tests were thus interpreted to obtain the hydraulic properties of the "karst facies" (Audouin and Bodin, 2008). The resulting transmissivity and storage coefficient values range from $5 \times 10^{-3}\,m^2\,s^{-1}$ to $8 \times 10^{-2}\,m^2\,s^{-1}$ and from 1×10^{-10} to 5×10^{-5}. Based on the interpretations of the two data sets described above, the hydraulic properties of the "non-karstified rock facies" may be derived by seeking transmissivity and storativity values consistent with (i) the bulk transmissivity and storage properties of the karst-matrix system as assessed from the pumping test data and assumed to correspond to geometric and

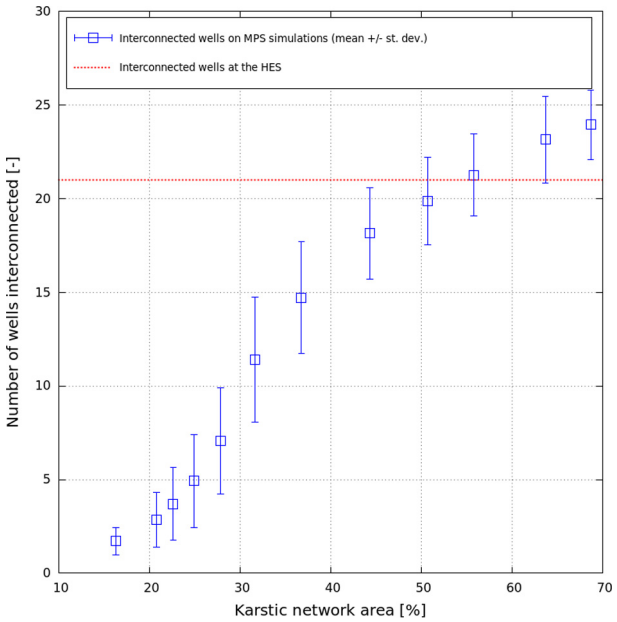

Fig. 6. Relationship between the proportion of karst networks and the number of interconnected wells for a total of 25 wells located as illustrated in Fig. 2(b). A set of 100 MPS realizations was used for each tested proportion.

arithmetic means, respectively, and (ii) the "karst facies" hydraulic properties as assessed from the slug test data (Table 1).

3.3. Numerical framework

A 2D uniform grid of unit thickness was superimposed on the simulated karst network images for the mapping of hydraulic properties and for subsequent flow simulations using the code MODFLOW-2005 (Harbaugh, 2005). The overall size of the grid was 500 m × 500 m, and its resolution was chosen to be identical to that of the MPS simulations, namely, 1 m × 1 m. Depending on whether it matched with the with MPS-simulated karst conduit elements, each MODFLOW cell was assigned to hydraulic properties selected either within the "karst facies" or "non-karstified rock facies" range values discussed in Section 3.2.

To minimize boundary effects, this domain was assumed to be surrounded by a homogeneous zone with the hydraulic properties of the bulk aquifer material, extending 700 m in each horizontal direction, with grid elements increasing in size from 1 m to 25 m. A homogeneous fixed head value was set at the limits of the domain. To consider the vertical leakance from the limestone matrix layers interbedded with the karst horizons, a uniform grid layer (of unit thickness) with the hydraulic properties of the porous matrix was added to the initial two-dimensional grid.

The numerical code MODFLOW-2005 (Harbaugh, 2005) was used to simulate the pumping test experiments by considering various sets of hydraulic properties and various karst network images.

4. Simulation investigations

Two series of simulations were performed to answer the following questions. Does the proposed modeling approach allow the reproduction of the specific hydraulic behaviors observed during the HES pumping test experiments? How could these behaviors be explained by the structural properties of the karst network? How do local changes in either the hydraulic properties or the karst network structure affect the drawdown responses?

4.1. Test #1

The purpose of Test #1 was to assess the ability of the proposed approach to reproduce the hydraulic behaviors observed during the HES pumping test experiments. Pumping with a rate of 2×10^{-2} m^3 s^{-1} over a period of 1×10^4 s was simulated within the karst network at the center of the domain, and the resulting drawdowns were recorded at 24 observation wells in locations consistent with the HES well arrangement (Fig. 2(b)). This simula-

Table 1
Tested and selected transmissivities (T) and storage coefficients (S) for the facies under interest.

Facies	Property	Tested range (Test #1)	Selected value (Test #2)
Karst	T (m^2 s^{-1})	5×10^{-3}–8×10^{-2}	5×10^{-2}
	S (–)	1×10^{-10}–5×10^{-5}	5×10^{-5}
Non-karstified rock	T (m^2 s^{-1})	–	1×10^{-6}
	S (–)	–	1×10^{-3}
Bulk aquifer (surrounding homogeneous zone)	T (m^2 s^{-1})	6×10^{-4}–3×10^{-2}	4×10^{-4}
	S (–)	4×10^{-5}–3×10^{-1}	5×10^{-4}

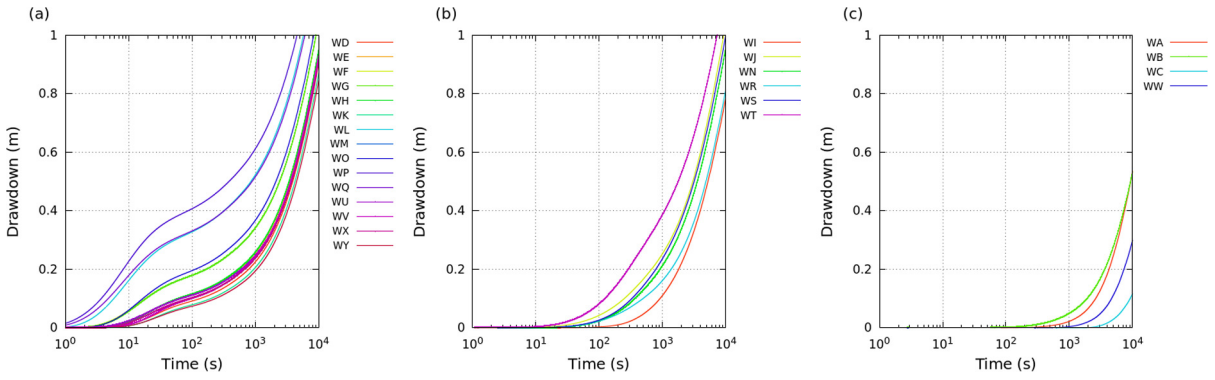

Fig. 7. Simulated drawdown responses during a pumping-test experiment at the center of the domain (Well M): hydraulic behaviors 1 (a), 2 (b) and 3 (c).

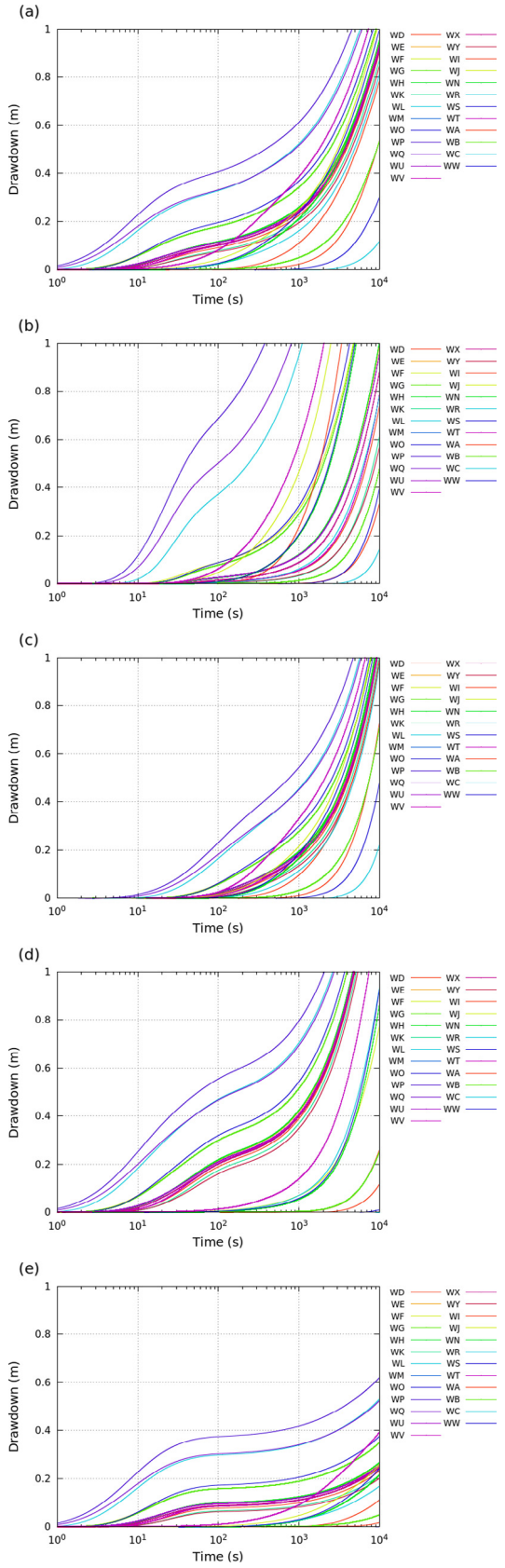

Fig. 8. Simulated drawdown responses during a pumping-test experiment at the center of the domain (Well M) using various hydraulic property sets: selected values, see Sect. 4.1. (a), lower transmissivity for the karst facies (5×10^{-3} m^2 s^{-1}) (b), higher storage coefficient for the karst facies (5×10^{-4}) (c), lower transmissivity for the matrix facies (1×10^{-7} m^2 s^{-1}) (d) and higher storage coefficient for the matrix facies (1×10^{-2}) (e).

tion was repeated for 100 sets of hydraulic properties randomly sampled from uniform distributions constructed from the ranges established in Section 3 (Table 1). A single MPS-simulated karst network image with a karst proportion of 55% was used throughout the entire experiment. The MPS realization used is illustrated in Fig. 5(d).

By qualitatively analyzing the drawdown curves, hydraulic properties that result in behaviors consistent with those discussed in Section 2.2 were identified. Hence, with transmissivity and storage coefficient values of, respectively, 4×10^{-4} m^2 s^{-1} and 5×10^{-4} for the outer bulk material, 5×10^{-2} m^2 s^{-1} and 5×10^{-5} for the karst facies and, 1×10^{-6} m^2 s^{-1} and 1×10^{-3} for the porous matrix facies, the following behaviors were generated: (i) at 14 observation wells (Fig. 7(a)), inflection of the drawdown curves occurs between 10 and 100 s, and the drawdown curves are close in both time and amplitude at intermediate times (10^3–10^4 s) (behavior 1); (ii) at six observation wells (Fig. 7(b)), no inflection occurs at early times, and the drawdown curves are similar to the previous ones in time and amplitude at intermediate times (behavior 2); (iii) at four observation wells (Fig. 7(c)), no inflection occurs, and the arrival time is significantly delayed (by approximately 10^3 s) with respect to the other observation wells (behavior 3); and (iv) at all observation wells, the drawdown curves are convex at intermediate times.

The main effects of changes in the hydraulic property values are (i) a wider spread of the drawdown values at a given time when the transmissivity of the karst facies is decreased (Fig. 8(b) vs. 8 (a)), (ii) delayed arrival times of the drawdown signals when the storage coefficient of the karst facies is increased (Fig. 8(c) vs. 8 (a)), (iii) steeper slopes of the drawdown curves at early times when the transmissivity of the porous matrix facies is decreased (Fig. 8(d) vs. 8(a)), and (iv) decreased slopes of the drawdown curves at intermediate times when the storage coefficient of the porous matrix facies is increased (Fig. 8(e) vs. 8(a)).

4.2. Test #2

The purpose of Test #2 was to assess the influence of the karst network geometry on the drawdown responses. A pumping test similar to Test #1 was simulated, but rather than considering a single karst network geometry and varying the hydraulic properties of

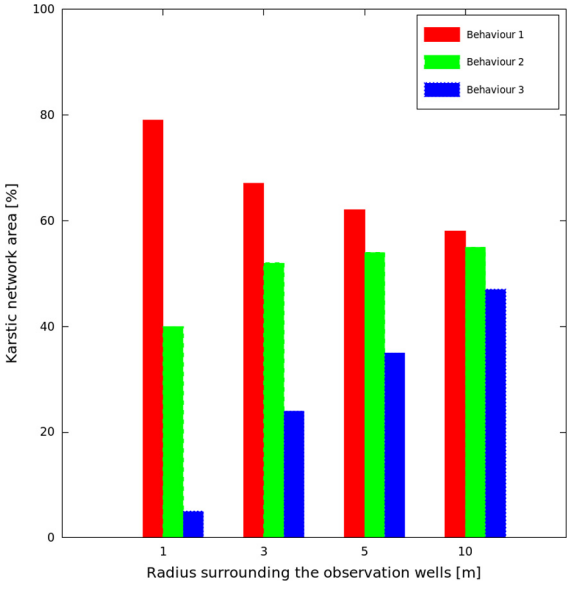

Fig. 9. Mean proportions of karst facies surrounding observation wells associated with a given hydraulic head behavior (statistics based on 100 MPS-groundwater simulations).

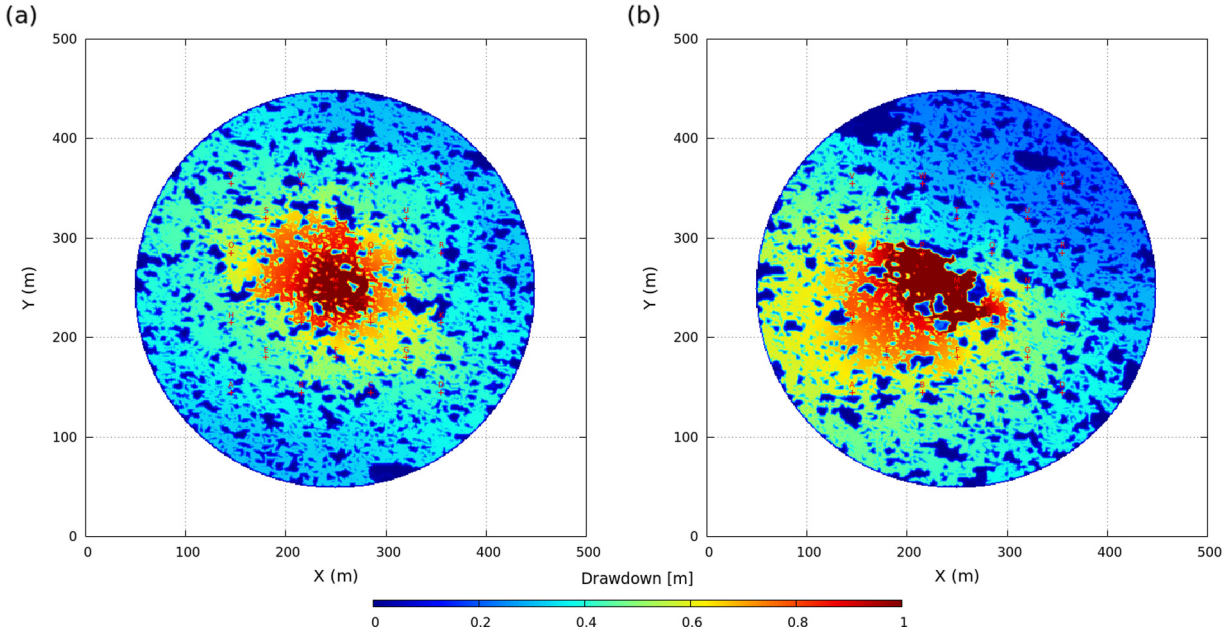

Fig. 10. Examples of drawdown surfaces (for a pumping rate of 2×10^{-2} m^3 s^{-1} at the center of the domain over a period of 1×10^4 s) simulated for a well-developed (a) and poorly developed (b) karst network close to the pumping well.

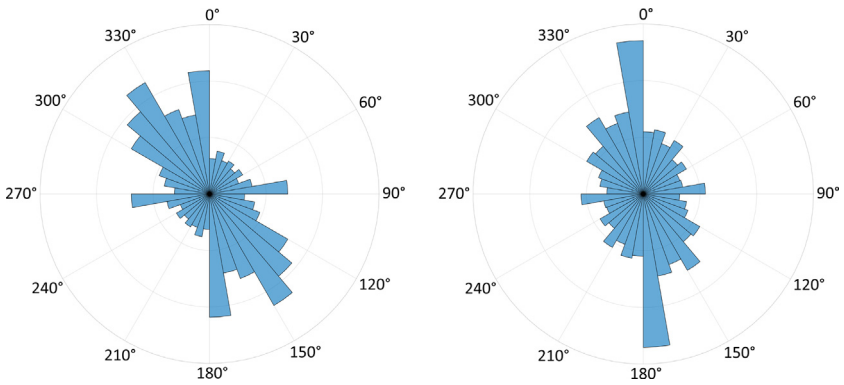

Fig. 11. Distribution of preferential karst directions in the training image (left) and the MPS realizations (right), obtained using the plugin "Directionality" of the software ImageJ/Fiji (http://imagej.net/Directionality).

the three facies between the simulations, the sets of hydraulic properties were held constant and the flow simulations were repeated using 100 MPS-simulated karst network images with a karst proportion of 55%. The set of hydraulic properties identified from Test #1 as resulting in hydraulic behaviors consistent with those observed at the HES was used throughout the entire experiment (Table 1).

The three types of behavior previously described were reproduced in every simulation. Behaviors 1 (mean number of wells: 6) and 2 (mean number of wells: 13) are characteristic of wells that intersect a karst network or that are located within the porous matrix close to a karst channel. A more detailed analysis (Fig. 9) accounting for the karst network proportion surrounding the wells indicates that behavior 1 generally corresponds to wells located within sub-areas with a relatively high karst network proportion compared with the wells that exhibit behavior 2: for a radius of 3 m surrounding the observation well, the mean karst proportion is 67% for behavior 1 and 52% for behavior 2, whereas for a radius of 10 m, the mean karst proportion is 58% for behavior 1 and 55% for behavior 2. Behavior 3 (mean number of wells: 5) is characteristic of wells isolated within the porous matrix. The delay in arrival time increases with increasing distance between the well and the closest karst channel.

In most cases, the drawdown signal appears to propagate preferentially in the NW-SE direction (Fig. 10(a)), which also corresponds to the predominant direction of the karst features mapped in the MPS training image (Fig. 5(a)). For karst networks that are poorly developed at the center of the domain, the cone of depression can be spatially deformed (Fig. 10(b)) while generally preserving the different hydraulic behaviors. The hydraulic response of a given observation well in terms of both behavior (1 or 2) and amplitude can therefore vary depending on the local configuration of the karst network close to the pumping well.

The preferential propagation of simulated drawdowns along the NW-SE direction suggests that despite the use of a non-stationary training image, the main karst directions have actually been preserved from the training image to the MPS realizations. In order to verify this conjecture, both the training image and a set of MPS realizations were analyzed with the plugin "Directionality" of the image processing software ImageJ/Fiji (http://imagej.net/Directionality). As shown in Fig. 11, the preferred karst orientations, namely N140°, N170°, and N80°, are similar between the

training image and the MPS realizations although characterized by different relative proportions.

5. Summary and discussion

The modeling approach adopted in this study, which considers the influence of the spatial variability of hydrofacies through an explicit description of medium-scale heterogeneities, results in successful simulations of the main hydraulic behaviors observed during pumping test experiments performed at the HES, at least qualitatively. In the context of densely developed karst networks, the use of MPS therefore appears to be particularly interesting. Indeed, the structure of these karst networks at various scales is critical with regard to the propagation of the depletion wave induced by pumping.

For a given pumping test experiment, the early-time drawdown responses differ for different observation wells. In particular, although both oscillatory behavior and inflection of the signal occur at the majority of the observation wells, certain wells exhibit a regular increase in drawdown or a significant delay in the arrival time of the drawdown signal. Obviously, because the numerical flow model used in the present work does not account for inertial effects, the drawdown oscillations at early times cannot be reproduced (Butler and Zhan, 2004). However, the inflection of the signal is reproduced, with the exception of certain wells, consistent with field data. Simulations show that inflection occurs only at wells that are located in sub-areas of relatively high karst density. The local configuration of the karst network in the vicinity of the observation well is also crucial for wells that do not intersect with the network. The relative ‘‘isolation’’ of these wells within the porous matrix results in a marked delay in the arrival time of the drawdown signal. In addition, the simulations highlight the sensitivity of the model to the karst density in the vicinity of the pumping well. When the karst density surrounding a pumping well is high, the drawdown signal tends to propagate homogeneously in space, and the inverse also holds.

Our results show that although used beyond its original assumptions (and limitations), the MPS method enables the simulation of karst conduit networks that, if not closely resembling the training image, allows the complex hydraulic behavior of the HES aquifer to be captured. This finding broadens the potential applicability of the MPS method for the simulation of aquifer heterogeneities. However, the behavior observed at well M06, which is characterized by both higher drawdown values at the closest observation wells and a delay in the early-time inflections, was not reproduced. As indicated by the results of Test #1, this could be interpreted as indicative of a lower transmissivity and higher storage coefficient of the karst network because of, e.g., local variations in medium structure or properties.

6. Conclusion

Within the framework of groundwater flow modeling, MPS enables the consideration of an explicit and realistic description of the spatial structures induced by medium heterogeneities and the testing of the influence of such structures on aquifer hydraulic responses through a large number of realizations with fixed or variable lithofacies proportions. This study demonstrated that for the HES karstified limestone aquifer, an explicit and realistic representation of karst networks results in more consistent hydraulic behavior simulations than those previously obtained using continuum, hybrid and discrete approaches (Bodin et al., 2012). Moreover, the most critical structures controlling the hydraulic responses were identified, namely, (i) local variations in the karst proportion close to both the pumping and observation wells; (ii) the interwell connectivity at the field scale; and (iii) the overall geometry and orientation of the karst networks.

Although the MPS realizations afforded satisfactory results in terms of hydraulic behaviors, the approach developed in the present work is purely qualitative and needs to be better constrained with regard to the site of interest. Lithofacies conditioning based on hard connectivity data, e.g., the presence of a highly diffusive path connecting two specific wells, using an MPS algorithm that allows connectivity metrics to be taken into account (Renard et al., 2011) and the use of the large amount of geophysical information available at the HES as soft data to better constrain the MPS computations are among the most promising potential methods for reducing the discrepancy between the simulated and observed drawdowns at a given well.

The calibration of specific well responses to groundwater flow experiments is a very important next step in the application of the MPS method to groundwater flow modeling. The main challenge is the coupling of MPS and inverse modeling algorithms for the optimization of spatially-distributed model parameters through the minimization of an objective function integrating time-variant and spatially-distributed drawdowns. This topic is currently an active research area, but, to the best of our knowledge, no satisfactory coupling strategy has yet been reported. According to a recent review by Linde et al. (2015), possible strategies include the use of Markov Chain Monte Carlo (MCMC) sampling methods or Probability Perturbation Methods (PPM). The main limitation of the first approach is the excessive computational time (i.e. slow convergence) caused by the random nature of the method, which makes it impractical for real field-scale problems. For the second approach, the main issue is the discontinuity of the objective function with respect to the perturbation parameter. Such discontinuity may occur when high or low hydraulic conductivity structures are suddenly connected or disconnected during the iteration process (Alcolea and Renard, 2010). Another key challenge pointed out by Ronayne et al. (2008) was the progress towards the identification of information content from transient drawdown data. The present study uniquely contributes to this topic by showing how the drawdown response at a particular location depends on the local karst proportion and induced inter-well connectivity. Put another way, it is possible to infer the local configuration of the karst conduit system from the drawdown response behavior at a particular location. A possible strategy is therefore to swap between ‘‘well-suited” training images depending on the drawdown behavior signature of a given observation well. This local training image will be used for simulating local MPS karst networks around the well. Because real-world training images may not exist for the whole range of targeted behaviors, the idea is to generate ‘‘pseudo training images” by subsetting initial sets of MPS realizations corresponding to different karst densities. Such approach will be explored in a future work.

Acknowledgements

This work was supported by the National Research Observatory H+. The assistance of Julien Straubhaar in using Impala is gratefully acknowledged. We thank the ‘‘Comité Départemental Spéléologique de la Vienne” for providing the map of the Cuchon cavern.

Appendix A. Supplementary material

Supplementary data associated with this article can be found, in the online version, at http://dx.doi.org/10.1016/j.jhydrol.2016.12.010. These data include Google maps of the most important areas described in this article.

References

Alcolea, A., Renard, P., 2010. Blocking Moving Window algorithm: Conditioning multiple-point simulations to hydrogeological data. Water Resour. Res. 46, W08511. http://dx.doi.org/10.1029/2009WR007943.

Allard, D., Comunian, A., Renard, P., 2012. Probability aggregation methods in geoscience. Math. Geosci. 44 (5), 545–581. http://dx.doi.org/10.1007/s11004-012-9396-3.

Audouin, O., Bodin, J., Porel, G., Bourbiaux, B., 2008. Flowpath structure in a limestone aquifer: multi-borehole logging investigations at the hydrogeological experimental site of Poitiers. France. Hydrogeol. J. 16 (5), 939–950. http://dx.doi.org/10.1007/s10040-008-0275-4.

Audouin, O., Bodin, J., 2008. Cross-borehole slug test analysis in a fractured limestone aquifer. J. Hydrol. 348 (34), 510–523. http://dx.doi.org/10.1016/j.jhydrol.2007.10.021.

Balan, S.E., 2012. Characterization and modeling of paleokarst reservoirs using multiple-point statistics on a non-gridded basis. PhD thesis, The University of Texas at Austin.

Bernard, S., Delay, F., Porel, G., 2006. A new method of data inversion for the identification of fractal characteristics and homogenization scale from hydraulic pumping tests in fractured aquifers. J. Hydrol. 328 (3–4), 647–658. http://dx.doi.org/10.1016/j.jhydrol.2006.01.008.

Bianchi, M., Kearsey, T., Kingdon, A., 2015. Integrating deterministic lithostratigraphic models in stochastic realizations of subsurface heterogeneity. Impact on predictions of lithology, hydraulic heads and groundwater fluxes. J. Hydrol. 531 (3), 557–573. http://dx.doi.org/10.1016/j.jhydrol.2015.10.072.

Bodin, J., Ackerer, P., Boisson, A., Bourbiaux, B., Bruel, D., de Dreuzy, J.R., Delay, F., Porel, G., Pourpak, H., 2012. Predictive modelling of hydraulic head responses to dipole flow experiments in a fractured/karstified limestone aquifer: Insights from a comparison of five modelling approaches to real-field experiments. J. Hydrol. 454, 82–100. http://dx.doi.org/10.1016/j.jhydrol.2012.05.069.

Borghi, A., Renard, P., Jenni, S., 2012. A pseudo-genetic stochastic model to generate karstic networks. J. Hydrol. 414, 516–529. http://dx.doi.org/10.1016/j.jhydrol.2011.11.032.

Butler, J.J., Zhan, X., 2004. Hydraulic tests in highly permeable aquifers. Water Resour. Res. 40 (12). http://dx.doi.org/10.1029/2003WR002998.

Chatelier, M., Ruelleu, S., Bour, O., Porel, G., Delay, F., 2011. Combined fluid temperature and flow logging for the characterization of hydraulic structure in a fractured karst aquifer. J. Hydrol. 400 (34), 377–386. http://dx.doi.org/10.1016/j.jhydrol.2011.01.051.

Chugunova, T.L., Hu, L.Y., 2008. Multiple-point simulations constrained by continuous auxiliary data. Math. Geosci. 40 (2), 133–146. http://dx.doi.org/10.1007/s11004-007-9142-4.

dell'Arciprete, D., Bersezio, R., Felletti, F., Giudici, M., Comunian, A., Renard, P., 2012. Comparison of three geostatistical methods for hydrofacies simulation: a test on alluvial sediments. Hydrogeol. J. 20 (2), 299–311. http://dx.doi.org/10.1007/s10040-011-0808-0.

dell'Arciprete, D., Vassena, C., Baratelli, F., Giudici, M., Bersezio, R., Felletti, F., 2014. Connectivity and single/dual domain transport models: tests on a point-bar/channel aquifer analogue. Hydrogeol. J. 22 (4), 761–778. http://dx.doi.org/10.1007/s10040-014-1105-5.

Filipponi, M., Jeannin, P.Y., Tacher, L., 2009. Evidence of inception horizons in karst conduit networks. Geomorphology 106 (12), 86–99. http://dx.doi.org/10.1016/j.geomorph.2008.09.010.

Fournillon, A., Viseur, S., Arfib, B., Borgomano, J., 2010. Insights of 3D geological modelling in distributed hydrogeological models of karstic carbonate aquifers. In: Andreo, B., Carrasco, F., Durn, J.J., LaMoreaux, J.W. (Eds.), Advances in Research in Karst Media, Environmental Earth Sciences. Springer, Berlin Heidelberg, pp. 257–262.

Harbaugh, A., 2005. MODFLOW-2005, the U.S. Geological Survey Modular Ground Water Flow Model – The Groundwater Flow Process. Technical report, Techniques and Methods 6–A16 U.S. Geological Survey, Reston, Virginia.

Huysmans, M., Dassargues, A., 2011. Direct multiple-point geostatistical simulation of edge properties for modeling thin irregularly shaped surfaces. Math. Geosci. 43 (5), 521–536. http://dx.doi.org/10.1007/s11004-011-9336-7.

Huysmans, M., Dassargues, A., 2012. Modeling the effect of clay drapes on pumping test response in a cross-bedded aquifer using multiple-point geostatistics. J. Hydrol. 450–451 (11), 159–167. http://dx.doi.org/10.1016/j.jhydrol.2012.05.014.

Kaczmaryk, A., Delay, F., 2007a. Improving dual-porosity-medium approaches to account for karstic flow in a fractured limestone: Application to the automatic inversion of hydraulic interference tests (Hydrogeological Experimental Site, HES, Poitiers, France). J. Hydrol. 347 (3–4), 391–403. http://dx.doi.org/10.1016/j.jhydrol.2007.09.027.

Kaczmaryk, A., Delay, F., 2007b. Interference pumping tests in a fractured limestone (Poitiers, France): Inversion of data by means of dual-medium approaches. J. Hydrol. 337 (1–2), 133–146. http://dx.doi.org/10.1016/j.jhydrol.2007.01.025.

Kaufmann, G., Braun, J., 2000. Karst aquifer evolution in fractured, porous rocks. Water Resour. Res. 36 (6), 1381–1391. http://dx.doi.org/10.1029/1999WR900356.

Knudby, C., Carrera, J., 2006. On the use of apparent hydraulic diffusivity as an indicator of connectivity. J. Hydrol. 329 (3–4), 377–389. http://dx.doi.org/10.1016/j.jhydrol.2006.02.026.

Le Coz, M., Genthon, P., Adler, P.M., 2011. Multiple-point statistics for modeling facies heterogeneities in a porous medium: the Komadugu-Yobe alluvium. Lake Chad Basin. Math. Geosci. 43 (7), 861–878. http://dx.doi.org/10.1007/s11004-011-9353-6.

Lee, J., Kitanidis, P.K., 2013. Bayesian inversion with total variation prior for discrete geologic structure identification. Water Resour. Res. 49 (11), 7658–7669. http://dx.doi.org/10.1002/2012WR013431.

Linde, N., Renard, P., Mukerj, T., Caers, J., 2015. Geological realism in hydrogeological and geophysical inverse modeling: A review. Adv. Water Resour. 86 (A), 86–101. http://dx.doi.org/10.1016/j.advwatres.2015.09.019.

Mari, J.L., Porel, G., 2008. 3D seismic imaging of a near-surface heterogeneous aquifer: A case study. Oil & Gas Science and Technology – Rev. IFP Energies Nouvelles 63 (2), 179–201. http://dx.doi.org/10.2516/ogst:2007077.

Mari, J.L., Porel, G., Bourbiaux, B., 2009. From 3D seismic to 3D reservoir deterministic model thanks to logging data: the case study of a near surface heterogeneous aquifer. Oil & Gas Science and Technology – Rev. IFP Energies Nouvelles 64 (2), 119–131. http://dx.doi.org/10.2516/ogst/2008049.

Noushabadi, M.R.J., Jourde, H., Massonnat, G., 2011. Influence of the observation scale on permeability estimation at local and regional scales through well tests in a fractured and karstic aquifer (Lez aquifer, Southern France). J. Hydrol. 403 (3–4), 321–336. http://dx.doi.org/10.1016/j.jhydrol.2011.04.013.

Renard, P., Allard, D., 2013. Connectivity metrics for subsurface flow and transport. Adv. Water Resour. 51, 168–196. http://dx.doi.org/10.1016/j.advwatres.2011.12.001.

Renard, P., Straubhaar, J., Caers, J., Mariethoz, G., 2011. Conditioning facies simulations with connectivity data. Math. Geosci. 43 (8), 879–903. http://dx.doi.org/10.1007/s11004-011-9363-4.

Ronayne, M.J., Gorelick, S.M., Caers, J., 2008. Identifying discrete geologic structures that produce anomalous hydraulic response: an inverse modeling approach. Water Resour. Res. 44 (8). http://dx.doi.org/10.1029/2007WR006635.

Straubhaar, J., Renard, P., Mariethoz, G., Froidevaux, R., Besson, O., 2011. An improved parallel multiple-point algorithm using a list approach. Math. Geosci. 43 (3), 305–328. http://dx.doi.org/10.1007/s11004-011-9328-7.

Strebelle, S., 2002. Conditional simulation of complex geological structures using multiple-point statistics. Math. Geol. 34 (1), 1–21. http://dx.doi.org/10.1023/A:1014009426274.

Strebelle, S., Zhang, T., 2005. Non-Stationary Multiple-point Geostatistical Models. In: Leuangthong, O., Deutsch, C.V. (Eds.), Geostatistics Banff 2004. Springer, Dordrecht, pp. 235–244.